4. CONCLUSIONS

We have described the construction of four different realistic breast phantoms, each representing a different volumetric breast density classification. The phantoms were constructed using TM materials that accurately represent the dielectric properties of various breast tissues. The phantoms were heterogeneous, each with a skin layer and a complex network of fibroglandular and fatty tissues. We verified the integrity of the internal structure of the phantom by obtaining CT images. The dielectric properties of the phantom constituents were verified by cutting the phantoms in half and measuring the dielectric properties of the phantom cross-section. These phantoms were constructed using simple techniques and have long term stability when not exposed to air for long periods of time. The techniques described here may be easily modified to construct phantoms with malignant lesions.

ACKNOWLEDGMENTS

The authors thank Christine Jaskowiak (University of Wisconsin, School of Medicine and Public Health) for her assistance in obtaining the CT images. This work was supported by the Department of Defense Breast Cancer Research Program under grant W81XWH-07-1-0629 and the National Institutes of Health under grant R01CA112398 awarded by the National Cancer Institute.

REFERENCES

1. M. Lazebnik, E.L. Madsen, G.R. Frank, and S.C. Hagness, Tissue-mimicking phantom materials for narrowband and ultrawideband microwave applications, Phys Med Biol 50 (2005), 4245–4258.
2. M. Lazebnik, L. McCartney, D. Popovic, C.B. Watkins, M.J. Lindstrom, J. Harter, S. Sewall, A. Magliocco, J.H. Booske, M. Okoniewski, and S.C. Hagness, A large-scale study of the ultrawideband microwave dielectric properties of normal breast tissue obtained from reduction surgeries, Phys Med Biol 52 (2007), 2637–2656.
3. K. Kerlikowske, L. Ichikawa, D.L. Miglioretti, D.S.M. Buist, P.M. Vacek, R. Smith-Bindman, B. Yankaskas, P.A. Carney, and R. Ballard-Barbash, Longitudinal measurement of clinical mammographic breast density to improve estimation of breast cancer risk, J Natl Cancer Inst 99 (2007), 386–395.
4. P.A. Carney, D.L. Miglioretti, B.C. Yankaskas, K. Kerlikowske, R. Rosenberg, and C.M. Rutter, Individual and combined effects of age, breast density, and hormone replacement therapy use on the accuracy of screening mammography, Ann Int Med 138 (2003), 168–175.
5. P.M. Meaney, N.K. Yagnamurthy, and K.D. Paulsen, Pre-scaled two-parameter Gauss-Newton image reconstruction to reduce property recovery imbalance, Phys Med Biol 47 (2002), 1101–1119.
6. D. Li, P.M. Meaney, T.D. Tosteson, S. Jiang, T.E. Kerner, T.O. McBride, B.W. Pogue, A. Hartov, and K.D. Paulsen, Comparisons of three alternative breast modalities in a common phantom imaging experiment, Med Phys 30 (2003), 2194–2205.
7. J.M. Sill and E.C. Fear, Tissue sensing adaptive radar for breast cancer detection—Experimental investigation of simple tumor models, IEEE Trans Microwave Theory Tech 53 (2005), 3312–3319.
8. D.W. Winters, J.D. Shea, E.L. Madsen, G.R. Frank, B.D. Van Veen, and S.C. Hagness, Estimating the breast surface using UWB microwave monostatic backscatter measurements, IEEE Trans Biomed Eng 55 (2008), 247–256.
9. M. Klemm, J.A. Leendertz, D. Gibbins, I.J. Craddock, A. Preece, and R. Benjamin, Microwave radar-based breast cancer detection: Imaging in inhomogeneous breast phantoms, IEEE Antennas Wireless Propag Lett 8 (2009), 1349–1352.
10. S.M. Salvador and G. Vecchi, Experimental tests of microwave breast cancer detection on phantoms, IEEE Trans Antennas Propag 57 (2009), 1705–1712.
11. M. Miyakawa, S. Takata, and K. Inotsume, Development of non-uniform breast phantom and its microwave imaging for tumor detection by CP-MCT, In: Proceedings of the Annual International Conference of the IEEE Engineering in Medicine and Biology Society, 2009, pp. 2723–2726.
12. J. Croteau, J. Sill, T. Williams, and E. Fear, Phantoms for testing radar-based microwave breast imaging, Presented at the 13th International Symposium on Antenna Technology and Applied Electromagnetics and Canadian Radio Sciences Meeting, 2009.
13. M. Ostadrahimi, R. Reopelle, S. Noghanian, S. Pistorius, A. Vahedi, and F. Safari, A heterogeneous breast phantom for microwave breast imaging, In: Proceedings of the Annual International Conference of the IEEE Engineering in Medicine and Biology Society, 2009, pp. 2727–2730.
14. A. Mashal, B. Sitharaman, X. Li, P.K. Avti, A.V. Sahakian, J.H. Booske, and S.C. Hagness, Toward carbon-nanotube-based theranostic agents for microwave detection and treatment of breast cancer: Enhanced dielectric and heating response of tissue-mimicking materials, IEEE Trans Biomed Eng 57 (2010), 1831–1834.
15. S. Gabriel, R.W. Lau, and C. Gabriel, The dielectric properties of biological tissues: III. Parametric models for the dielectric spectrum of tissues, Phys Med Biol 41 (1996), 2271–2293.
16. D. Popovic, L. McCartney, C. Beasley, M. Lazebnik, M. Okoniewski, S.C. Hagness, and J.H. Booske, Precision open-ended coaxial probes for in vivo and ex vivo dielectric spectroscopy of biological tissues at microwave frequencies, IEEE Trans Microwave Theory Tech 53 (2005), 1713–1722.

DESIGN OF A HIGH-RESOLUTION MICROFLUIDIC MICROWAVE MEMS PHASE SHIFTER

Burak Ozbey, Sule Ozturk, and Ozgur Aktas
Department of Electrical and Electronics Engineering, Bilkent University, Bilkent, Ankara, Turkey; Corresponding author: aktas@ee.bilkent.edu.tr

Received 12 November 2010

ABSTRACT: *In this article, a novel microwave microelectromechanical phase shifter based on a microfluidic design is proposed and demonstrated. The design principles, the fabrication process, and experimental results (*S*-parameters and phase shift plots) are presented. The proposed system has a high bandwidth, high-power handling capacity, and a high-resolution along with a small settling time.* © 2011 Wiley Periodicals, Inc. Microwave Opt Technol Lett 53:1902–1905, 2011; View this article online at wileyonlinelibrary.com. DOI 10.1002/mop.26127

Key words: *MEMS; phase shifter; microfluidics*

1. INTRODUCTION

Microwave phase shifters are frequently used in communications and radar technology [1]. Recently, the need for phase shifters with low cost, high-power handling capacity, high resolution, and high bandwidth has made this topic an important research area in microwave engineering [2]. Although the traditional semiconductor and ferrite devices are also continuing to be used, there is an increasing trend of microelectromechanical (MEMS) phase shifters [2], which enable better characteristics in terms of power and loss.

Recently, several MEMS phase shifters operating in different bands of the microwave range have been shown [3–5]. These papers have shown devices based on the loaded-line or switched-line method [3] and also reflection method [4]. These

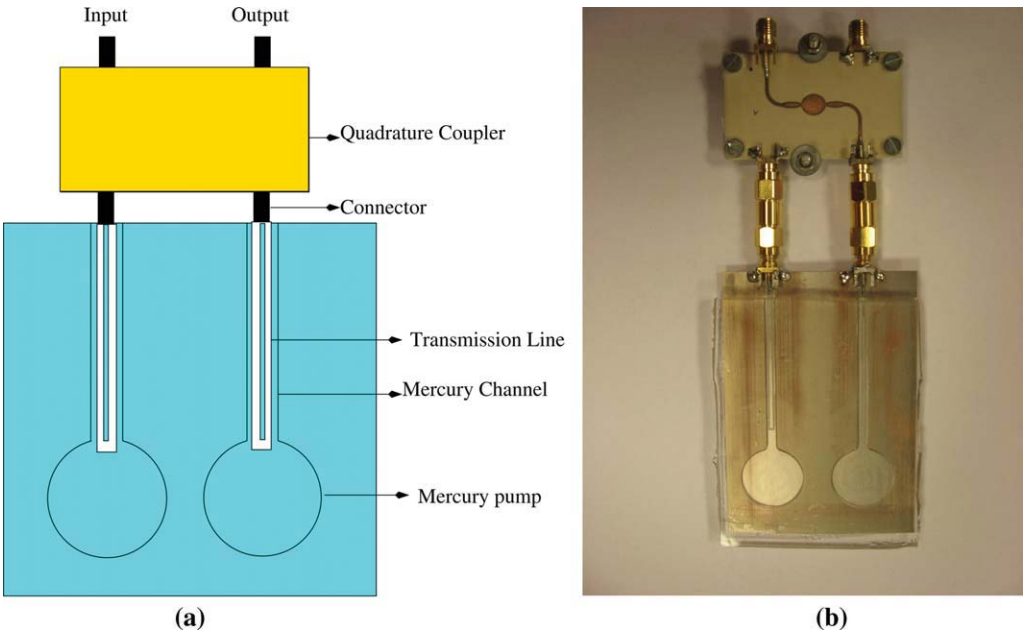

Figure 1 (a) Diagram of the complete system. (b) Photograph of the assembled system. [Color figure can be viewed in the online issue, which is available at wileyonlinelibrary.com]

approaches are based on MEMS switches, which are then used to either change the length of a transmission line connected to the system or the value of a capacitance or inductance at the end of a transmission line in discrete steps. As the number of various transmission line pieces, unit capacitors or inductors, and MEMS switches is limited, these approaches generally cannot achieve a high phase resolution.

Liquid microwave MEMS switches have been shown in the Refs. 6 and 7. However, the use of liquid metal MEMS systems has been limited only to switches. In this article, a novel MEMS phase shifter is proposed and demonstrated, which achieves high-power capacity together with high resolution by using a liquid metal approach and a microfluidic channel design. The design also has a high bandwidth and a high speed. The demonstrated MEMS microwave phase shifter is working in 2–6 GHz range. The design is based on reflection type phase shifting method and the shifter is able to present a phase shift of a desired degree (0–360 degrees) to the input signal with a high resolution. The bandwidth of the shifter is only limited by the coupler and the board material that is used and can be extended to a much greater value, and the resolution of the shifter is very high (nearly continuous phase shift). The power handling capacity is limited with the breakdown voltages of the transmission lines and other components, such as connectors, used in the design. The use of microfluidic design minimizes the mass and thus shortens the phase settling time. Although there is space for improvement on the loss characteristics, the main source of loss in the design was observed to be due to the microwave coupler instead of the main microfluidic channel structure. In this work, we present the steady state phase shift characteristics of the system at different frequencies measured under small signal conditions.

2. DESIGN

The shifter mainly consists of two parts: (1) Two parallel transmission lines in coplanar waveguide configuration with open termination at first which are covered with polydimethylsiloxane (PDMS) which forms two containers of mercury at the termination and also microchannels for the flow of mercury on the lines, and thus enables the whole system to behave as two sliding short-circuit stubs for the two transmission lines; (2) a wideband quadrature coupler which is connected to the transmision lines mentioned above. The system diagram and the photograph are shown in Figures 1(a) and 1(b), respectively.

The input to this system is the first port of the quadrature coupler, whereas the phase-shifted signal comes out of the isolated port. As mentioned above, the system uses the reflection typephase-shifting method, which is the same principle in [8], except that instead of the varactor diodes, two transmission lines whose lengths are changeable with the flow of mercury are connected to the through and coupled ports of the coupler in order to create the phase shift. The signals which are reflected from the transmission lines whose lengths are modulated by the flow of mercury are then combined at the isolated port forming the phase-shifted output signal. The reflected signals from the through and coupled ports combine destructively at the input port (with 180° of phase difference). The quadrature coupler design was based on the technique shown in [9], which demonstrates a high-bandwidth 3 dB quadrature coupler by Abbosh and Bialkowski.

There are several options for controlling the flow of mercury. In our system, it is achieved by a micropositioner which moves back and forth to increase or decrease the pressure applied to the mercury-filled container, and the position of mercury on the microchannel can then be set to the desired value by the movement of the micropositioner. Each position corresponds to a certain degree of phase shift, and the length of the transmission lines may be chosen such that a phase shift from 0 to 360 degrees can be obtained. For a 50 Ω grounded coplanar waveguide design on a 20-mil thick Rogers 4003 board, the parameters given below were used: W (width of the center conductor) $= 1.03$ mm, G (gap between the center conductor and the ground planes) $= 0.4$ mm. This corresponds to an effective relative permittivity $\varepsilon_{\text{eff}} = 2.47$; hence, at 2 GHz which is the lowest operating frequency, $\lambda_{\text{eff}} = 9.54$ cm. By considering that the

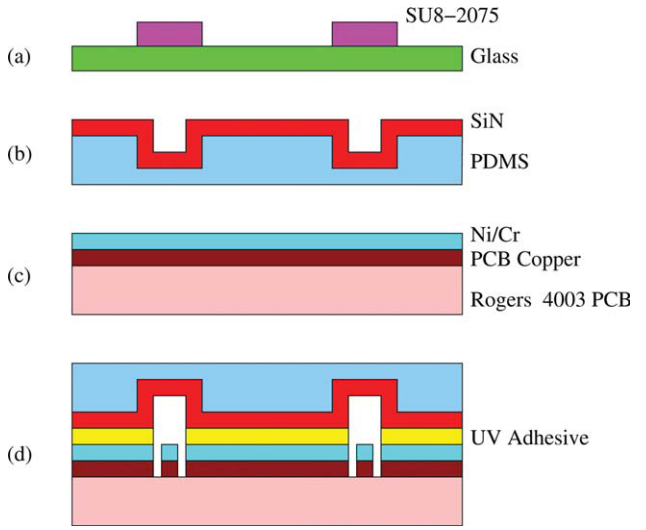

Figure 2 Cross sections of the device at various fabrication steps: (a) SU8 moulds used to form the PDMS microchannels. (b) PDMS microchannel coated with SiN. (c) Rogers 4003 PCB coated with NiCr. (d) The assembled system formed by combining (b) and (c) by a UV adhesive. [Color figure can be viewed in the online issue, which is available at wileyonlinelibrary.com]

reflected wave will travel the same distance twice, it is then found out that the minimum length of the transmission line should be 9.54/2 = 4.77 cm for 360 degrees of phase shift. At higher frequencies, smaller distances will be enough for a shift of 360 degrees.

3. FABRICATION

The fabrication process used in the design of microfluidic channels is described in Figure 2 and can be outlined as follows: First, the microchannels were formed on glass by lithography by using the SU8 2075. For this operation, the glass was first cleaned by acetone, methanol, and isopropanol, respectively, for 30 s. After keeping the glass in piranha, it was dried on a hotplate at 200°C for 10 min. Then the SU8 coating was performed by spinning at 500 rpm for 30 s. Afterward, the sample was baked at 100°C and then at 140°C. Temperature change rates were kept below 10°C/min both during heating and cooling of the sample. The mould was then exposed to UV for 20 min and then developed by MrDev 600 for 30 min making the mould ready for the next step.

Afterward, the microchannels were formed by pouring PDMS on to the mould. After PDMS was cured, it was peeled from the mould and coated with SiN to prevent the chemical reaction between mercury and PDMS. The sample was covered with 500-nm thick SiN by PECVD at 100°C. Furthermore, the mercury can also interact with the copper on RO4003 board. For preventing this, 80-nm-thick Ni-Cr was thermally evaporated under high vacuum to the surface of the PCB. After this, the NiCr coated PCB was used for the fabrication of the transmission lines. The transmission lines were etched to the surface using a LPKF Protomat S62 CNC miller.

Next, the SiN covered PDMS and Ni-Cr covered RO4003 PCB were bonded by using Norland Optical UV Adhesive. The sample was exposed to UV light from a 15 W black lamp for 4 h to achieve curing of the adhesive. Finally, same amount of mercury were injected into the microchannels for the measurements.

4. EXPERIMENT

The total additional phase shift versus the distance traveled by the mercury in vertical position, which is also equal to the length of the transmission line subtracted from the channel length is given in Figure 3.

The phase shift values displayed in Figure 3 are the phase shifts due to the change of the length of the transmission line connected to the coupler. The total phase shift experienced by the input signal is found by adding to this value the phase shift due to 343° at 2 GHz or 640° at 3.5 GHz.

In Figure 3, it can be seen that at 6 GHz, more than 2 full cycles of 360 degrees were achieved. At 2 GHz, a phase shift of 280 degrees is observed but with a slight extension of each of the transmission lines, this value can easily be transformed into 360 degrees. It can also be observed that the shifter is quite linear at lower frequencies and increasingly less linear as frequency increases. This can be attributed to the much more rapid change of the phase for the same distance as the wavelength is smaller, and the way the flow of mercury is controlled by the micropositioner. As the part of the shifter at which the tip of the micropositioner touches the container part of the microfluidic channel where mercury is stored is delicate and quite sensitive to the movements, a slight error in a single step of the micropositioner which is 10 mm means higher degrees of deviation and an increase in nonlinearity. On the other hand, nonlinearity is not a vital requirement because the movement of mercury on the microchannels is repeatable and each position of mercury corresponds to a certain level of additional phase shift. The resolution of the shifter is observed to be very high, providing a nearly continuous phase shift.

In Figure 4, the *S*-parameters of the MEMS phase shifter when the mercury level is 3 cm into the microchannel are shown. In Figure 5, the microchannel losses for the same level of mercury are shown.

S_{21}, the insertion loss of the phase shifter varies from 3 dB to over 30 dB in the 2–6 GHz range, but this is due to the imperfection in the design process of the coupler as in Figure 5, the losses in the microchannel are observed to be about 8–9 dB

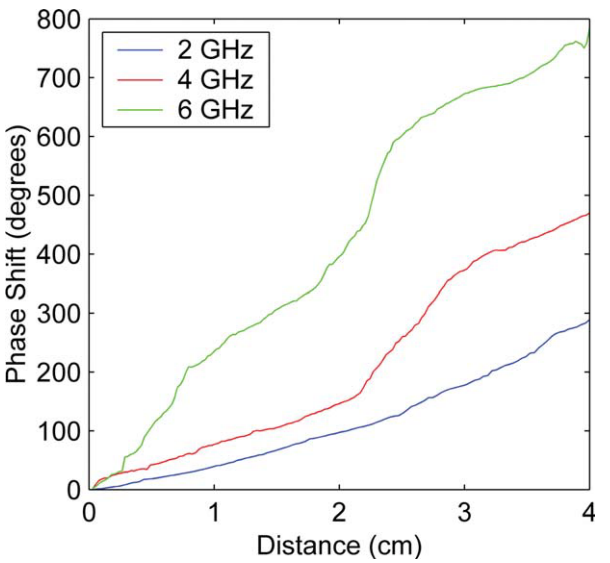

Figure 3 The total additional phase shift versus the distance traveled by the mercury at three separate frequencies: 2 GHz, 4 GHz, and 6 GHz. [Color figure can be viewed in the online issue, which is available at wileyonlinelibrary.com]

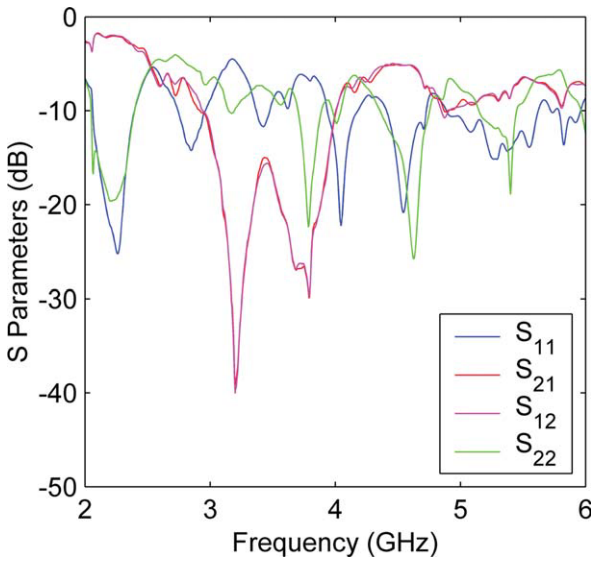

Figure 4 *S*-parameters of the MEMS phase shifter when the mercury level is 3 cm into the microchannel. [Color figure can be viewed in the online issue, which is available at wileyonlinelibrary.com]

at most. The losses of the microchannels specifically start to increase after 5 GHz especially for the first channel, but with proper changes and better fabrication of the microchannels, better loss characteristics can be obtained.

The effect of the depth of the microfluidic channels were also examined, and it was observed that the wider and deeper channels provide a smoother flow of mercury, thus enabling better performance in terms of linearity. Return losses, S_{11} and S_{22} of the shifter are observed to be below -5 dB for the whole range and below -10 dB for certain frequencies. However, wider and deeper channels translate to a larger mercury mass, which will reduce the mechanical resonant frequency and will likely increase the settling time between phase shift steps. It also needs to be mentioned that the settling time will be influenced by the resonances of the complete system and for low settling times a stiff design is required. Use of piezoelectric actuators, along with standard design principles to eliminate resonances will help accomplish this goal.

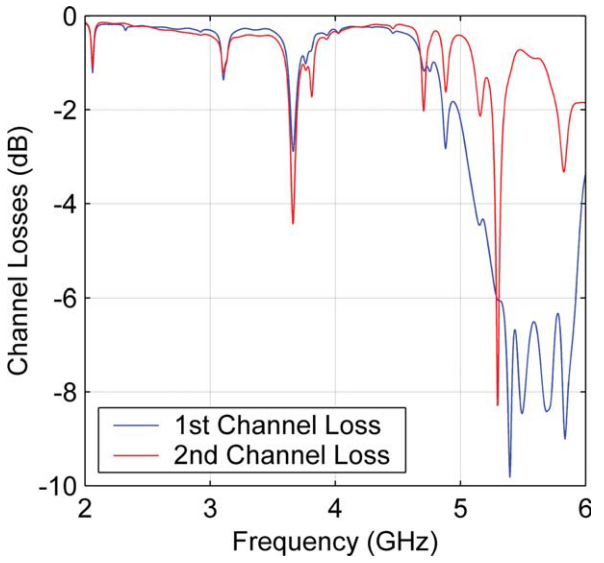

Figure 5 The microchannel losses when the mercury level is 3 cm into the microchannel. [Color figure can be viewed in the online issue, which is available at wileyonlinelibrary.com]

5. CONCLUSIONS

A novel microwave MEMS phase shifter based on microfluidic design has been proposed and demonstrated. *S*-parameters and phase shift values versus the change of the transmission line lengths were shown. The shifter is able to present 360 degrees of phase shift, and it has a high resolution, a high power handling capacity, and a theoretically high bandwidth that is limited by the quadrature coupler used in the design.

REFERENCES

1. N.S. Barker and G.M. Rebeiz, Optimization of distributed MEMS transmission-line phase shifters—u-band and w-band designs, IEEE Trans Microwave Theory Tech 48 (2000), 1957–1966.
2. T.S. Ji, K.J. Vinoy, and V.K. Varadan, Distributed MEMS phase shifters by microstereolithography on silicon substrates for microwave and millimeter wave applications, Smart Mater Struct 10 (2001), 1224–1229.
3. G.L. Tan, R.E. Mihailovich, J.B. Hacker, J.F. DeNatale, and G.M. Rebeiz, Low-loss 2-and 4-bit TTD MEMS phase shifters based on SP4T switches, IEEE Trans Microwave Theory Tech 51 (2003), 297–304.
4. A. Malczewski, S. Eshelman, B. Pillans, J. Ehmke, and C.L. Goldsmith, X-band RF MEMS phase shifters for phased array applications, IEEE Microwave Guided Wave Lett 9 (1999), 517–519.
5. B. Pillans, S. Eshelman, A. Malczewski, J. Ehmke, and C. Goldsmith, Ka-band RF MEMS phase shifters, IEEE Microwave Guided Wave Lett 9 (1999), 520–522.
6. C.H. Chen and D. Peroulis, Liquid RF MEMS wideband reflective and absorptive switches, IEEE Trans Microwave Theory Tech 55 (2007), 2919–2929.
7. P. Sen and C.J. Kim, A liquid-solid direct contact low-loss RF micro switch, J Microelectromech S 18 (2009), 990–997.
8. D.M. Krafcsik, S.A. Imhoff, D.E. Dawson, and A.L. Conti, A dual-varactor analog phase shifter operating at 6 to 18 GHz, IEEE Trans Microwave Theory Tech 36 (1988), 1938–1941.
9. A.M. Abbosh and M.E. Bialkowski, Design of ultra wideband 3dB quadrature microstrip/slot coupler, Microwave Opt Technol Lett 49 (2007), 2101–2103.

BROADBAND, HIGH GAIN SLOT LOADED SQUARE MICROSTRIP ARRAY ANTENNA

S. N. Mulgi and Kishan Singh
Department of PG Studies and Research in Applied Electronics, Gulbarga University, Gulbarga 585106, Karnataka, India;
Corresponding author: kishanskrish@gmail.com

Received 20 October 2010

ABSTRACT: *A novel two-element right angle slot loaded square microstrip array antenna (TESMAA) is presented for 52.18% of bandwidth and 11.22 dB of gain. The effect of different slots placed in the ground plane is studied for enhancing the bandwidth and gain. It is found that when bow-tie slot is placed in the ground plane of TESMAA the antenna gives maximum 95.54% of bandwidth and 15.92 dB of gain without affecting the nature of broad side radiation characteristics. The design concepts of antennas are described and experimental results are discussed.* © 2011 Wiley Periodicals, Inc. Microwave Opt Technol Lett 53:1905–1908, 2011; View this article online at wileyonlinelibrary.com. DOI 10.1002/mop.26110

Key words: *square microstrip array antenna; slot; bandwidth; gain*